

Group-wise 3D registration based templates to study the evolution of ant worker neuroanatomy

Ignacio Arganda-Carreras^{1,2,3}, Darcy G Gordon⁴, Sara Arganda^{4,5},
Maxime Beaudoin⁶, and James FA Traniello⁴

¹Ikerbasque, Basque Foundation for Science, Bilbao, Spain

²Dept. of Computer Science and Artificial Intelligence, Basque
Country University, San Sebastian, Spain

³Donostia International Physics Center (DIPC), San Sebastian,
Spain

⁴Department of Biology, Boston University, Boston,
Massachusetts, USA

⁵Centre de Recherches sur la Cognition Animale (CRCA), CNRS,
Toulouse, France

⁶Ecole d'Ingenieurs et Centre de Recherche (ENSTA), Bretagne,
France

Abstract

The evolutionary success of ants and other social insects is considered to be intrinsically linked to division of labor and emergent collective intelligence. The role of the brains of individual ants in generating these processes, however, is poorly understood. One genus of ant of special interest is *Pheidole*, which includes more than a thousand species, most of which are dimorphic, i.e. their colonies contain two subcastes of workers: minors and majors. Using confocal imaging and manual annotations, it has been demonstrated that minor and major workers of different ages of three species of *Pheidole* have distinct patterns of brain size and subregion scaling. However, these studies require laborious effort to quantify brain region volumes and are subject to potential bias. To address these issues, we propose a group-wise 3D registration approach to build for the first time bias-free brain atlases of intra- and inter-subcaste individuals and automatize the segmentation of new individuals.

1 Introduction

Ants (*Hymenoptera: Formicidae*), renowned for their remarkable diversity and ecological significance [1], typically display extraordinary collective behavior

[2]. A key question in evolutionary neurobiology concerns how ant sociality, ecology, and the ability to make accurate group decisions have impacted their brain structure. The emergence of eusociality and social complexity are major novelties likely involving rapid behavioural changes that might be reflected in the anatomy of the brain [3, 4].

The most generally accepted hypothesis explaining the great ecological success of ants relies on their striking social organization and collective behavior [5]. Ant colonies are so tightly interdependent that they are considered superorganisms. Individual brains must have evolved to cope with the multiple challenges of an increased sociality (communication, recognition, etc). The Social Brain Hypothesis, originally postulated on primates, postit that larger groups require bigger brains to adaptively process social information [6]. However, this might not apply to ants because as small-bodied insects, their brains must have evolved under restrictions of miniaturization. As eusocial insects, they show characteristics such as collective intelligence and division of labor, which may have relaxed the individual cognitive challenges, leading to reduced brain investment [7].

The ant brain is a mosaic of different subregions (neuropils) that correlate with identified functions [8]: sensory perception (antennal and optic lobes), motor control and navigation (central body and subesophageal ganglion), and multi-sensorial integration, learning and memory (mushroom bodies). Using confocal imaging and manual annotations of brain regions, Muscedere *et al.* demonstrated that minor and major workers of different ages of three species of *Pheidole* have distinct patterns of brain size variation [9]. These differences in subregion sizes and scales reflect the intra-colony division of labor and the socio-biological characteristics of this species. However, all these results come at the cost of allocating significant time to manual record the volumes of functionally specialized brain compartments, which can always introduce a potential bias.

Recent advances in image processing, inspired in techniques developed to study the human brain, have allowed extraordinary outputs of unprecedented quality and throughput in neuroanatomical studies in honeybees [10] and fruit flies [11]. These approaches combine multiple brains in a single model or template, which statistically represents the whole species. Performing replicates is necessary to avoid biases originated in the fixation and imaging processes of the brains as well as to account for inter-individual variability. Template brains have a dual function. On one hand, transforming all samples to the same reference space allows normalizing the information from brains imaged under different conditions or image modalities. On the other hand, the anatomical regions of the reference brains are usually annotated, which produces the automatic segmentation of the registered samples.

Although many strategies have been proposed and evaluated in the last decades for the construction of brain templates in mammals [12, 13, 14, 15, 16, 17], only a few of them have been applied to insect brains, most of them to *Drosophila* data [18, 19, 20, 21]. However, these results have not been translated yet into the ant brain community. This can be partially explained by the lack of expert-made anatomical labels and the larger morphological variability existing in the ant brain, what substantially hinders the registration process.

To address these issues, we propose a two-step co-registration solution that allows the construction of atlases of intra- and inter-caste individuals and identify specific differences between anatomical regions. Moreover, we have evaluated our approach in a total of 50 labeled brains of 4 different *Pheidole* species.

2 Materials and Methods

2.1 Ant brains dataset

2.1.1 Ant species

Pheidole, the most diverse and species rich ant genus [22], is characterized by worker polymorphism (minor worker, major workers and, in some species, supersoldiers). Four *Pheidole* species, courtesy of Dr. Diana Wheelers lab at the University of Arizona, have been selected for this study: *P. spadonia*, *P. rhea*, *P. tepicana* and *P. obtusospinosa*.

2.1.2 Brain imaging and labeling

The immunohistochemical staining and imaging of ant brain neuropil was slightly modified from [23, 9]. We imaged 50 brains at a resolution of $\sim 0.7 \times 0.7 \times 5\mu\text{m}/\text{voxel}$: 10 minor worker brains from the mentioned four species and 10 major worker brains from *P. spadonia*. Right brain hemispheres were manually labeled by an expert into 8 anatomical regions: optic lobes (OL), antennal lobes (AL), mushroom body medial calyx (MB-MC), mushroom body lateral calyx (MB-LC), mushroom body peduncle (MB-P), central body (CB), subesophageal ganglion (SEG) and rest of the brain (ROCB). Fig. 1 shows a 3D representation of the labels and brain samples of each type. (Image size: $\sim 600 \times 600 \times 80$ pixels.)

2.2 Image registration and template generation

Group-wise templates were constructed using an algorithm building an average shaped brain within the diffeomorphic space. The approach uses symmetric diffeomorphic image registration (SyN) [24] with mutual information and cross-correlation to register a group of brain images to one another. The co-registration process is refined using a two-step strategy. First, all of the images are registered to one brain using only an affine transformation model and mutual information as the similarity measure to optimize. The resulting images are then averaged to form an initial blurry reference brain image. Second, the original brain images are non-linearly registered to this average to create a new average that maximizes the cross-correlation of the intensities of all brains. In this second step, the registration is improved gradually at different (in our case, four) resolution levels and the result is an optimal average template.

For combining the co-registered images, we experimented first with a normalized voxel-wise average followed by sharpening with a Laplacian kernel (state-of-

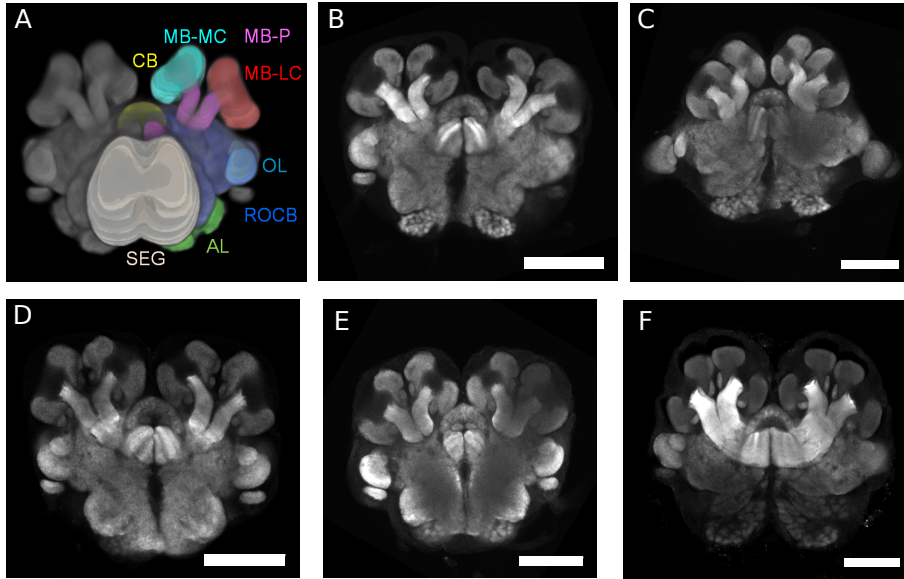


Figure 1: Examples of brain samples and labeled regions. From left to right and from top to bottom: 3D view of anatomical regions (A) and central sections of *P. spadonia minor* (B), *P. spadonia minor* (C), *P. tepicana* (D), *P. obtusospinosa* (E) and *P. rhea* (F) samples. Scale bar: $100\mu\text{m}$.

the-art in MRI). However, we found experimentally that an alternative strategy in which the template intensity image was generated by computing a voxel-wise median over the co-registered images produced slightly better results. The anatomical label image of the template was obtained by applying to each individual label image the diffeomorphic transformations computed from the corresponding confocal image, followed by a per-voxel majority voting over all warped label images.

Individual brain images were registered against the templates using the same two-step strategy, which performs an initial affine registration with mutual information as similarity metric followed by non-rigid registration with SyN and cross-correlation as similarity measure. The first registration is crucial in order to compensate for the large disparities in size among the different ant species and subcastes, while the second one locally finds an optimal solution. All methods are implemented within the Advanced Normalization Tools (ANTs) software [25].

2.3 Evaluation metrics

Using test brains, different templates were evaluated for their performances regarding segmentation. Thus, the template labels were transformed into the space of each individual test brain.

Region-to-region matching in individual space was quantified using the Dice coefficient. For any region R_i , the Dice coefficient provides a normalized measure of the overlap between two instances R_i^A and R_i^B that have been transformed into a common space by the registration procedure. The Dice coefficient is defined as

$$\text{Dice}(R_i) = 2 \frac{|R_i^A \cap R_i^B|}{|R_i^A| + |R_i^B|}$$

where $|\cdot|$ denotes volume.

The average boundary error, expressed in absolute distance units, was computed as the mean symmetric Euclidean distance. For region R_i , we computed the mean Euclidean distance $d_i^{A,B}$ between each boundary point on R_i^A and the closest point on R_i^B . The symmetric computation was performed to obtain $d_i^{B,A}$. The symmetric Euclidean distance for region R_i was then defined as

$$\text{Symmetric Euclidean distance}(R_i) = \frac{d_i^{A,B} + d_i^{B,A}}{2}$$

The maximum boundary error, also expressed in absolute distance units, was computed as the mean symmetric Hausdorff distance. For region R_i , the Hausdorff distance $h_i^{A,B}$ was computed as the maximum distance between any boundary point on R_i^A and its closest neighbor on R_i^B . The symmetric computation yielded $h_i^{B,A}$, and the symmetric Hausdorff distance was obtained as

$$\text{Symmetric Hausdorff distance}(R_i) = \frac{h_i^{A,B} + h_i^{B,A}}{2}$$

3 Results

3.1 Building an ant brain template

As a proof-of-concept of our methodology, we first attempted to build intra-species and intra-subcaste templates. For that reason, we chose the 10 minor and 10 major samples from *P. spadonia*. Here we realized that an initial affine pre-registration was needed due to the volume variability and imaging conditions. Both templates were successfully built and evaluated based on how well their consensus labels represented the sample population (see Fig. 2).

3.2 Building and evaluating hybrid templates

After analyzing the morphological differences of the sample populations based on their anatomical labels using the open-source toolbox MorphoLibJ [26] (see Fig. 3), we decided to build and evaluate hybrid templates mixing minor samples of the different species. More specifically, we constructed one template (RTO) using all minor species except *P. spadonia* (with 3 brains per species) and another template (SRTO) with *P. spadonia* samples as well. All samples not used as part of templates, were used for testing their performance. Fig. 4

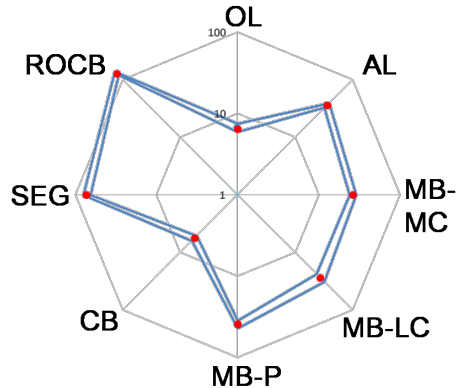


Figure 2: Evaluation of volume ($\times 10^4 \mu m^3$) per anatomical region of minor *P. spadonia* template. Blue lines represent the standard deviation of the volume of the original manual labels while the red dots are the template volume value.

shows the evaluation results per label for the 4 templates we created (*P. spadonia* major, *P. spadonia* minor, RTO and SRTO). The only template built with major samples performs notably worse than the other 3 using both overlap and distance metrics, specially in the OL and CB. It is remarkable how the *P. spadonia* minor performs only slightly worse than RTO and SRTO even though not a single *P. spadonia* sample was used for testing.

3.3 Evaluating dimorphisms

One advantage of having templates of a single type of brain is that they allow to study the main morphological differences between species and/or subcastes. Following a methodology previously contrasted for fly brains [11], we can register for instance our *P. spadonia* minor and major templates to each other, and calculate the volume change of each voxel via the use of the Jacobian determinant. Once the difference in size is compensated with the affine transform, the local non-linear deformations can be visualized as a heatmap (see Fig. 5), emphasizing the regions of large differences.

4 Conclusions and Future work

We have presented a groupwise 3D registration strategy to build bias-free ant brain atlases of intra- and inter-subcaste individuals and automatically segment new individuals. Moreover, we have numerically evaluated the performance of the atlases using expert-made manual annotations and shown that the templates can be used to study morphological inter- and intra-species differences. To the best of our knowledge, this is the first time that such an automation has been done to quantify ant brain volumes. The extension of the current work to a

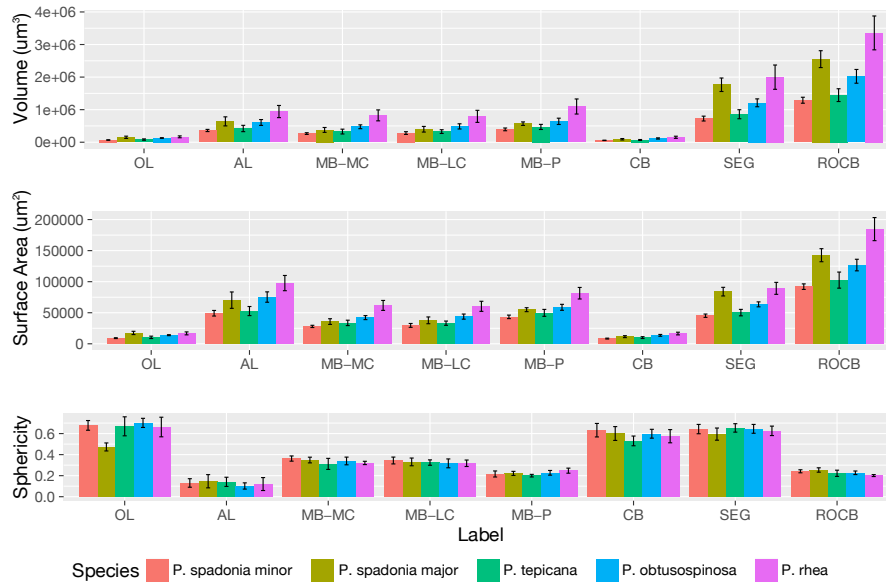


Figure 3: Morphological differences between species and subcastes. From top to bottom: volume, surface area and sphericity measurements.

much larger dataset will allow the study of the evolution of ant brain structure in relation to their ecological and evolutionary success and its basis in collective organization.

References

- [1] Edward O Wilson, *The diversity of life*, WW Norton & Company, 1999.
- [2] Bert Hölldobler and Edward O Wilson, *The superorganism: the beauty, elegance, and strangeness of insect societies*, WW Norton & Company, 2009.
- [3] Sarah M Farris, “Insect societies and the social brain,” *Current Opinion in Insect Science*, vol. 15, pp. 1–8, 2016.
- [4] Swidbert R Ott and Stephen M Rogers, “Gregarious desert locusts have substantially larger brains with altered proportions compared with the solitary phase,” *Proceedings of the Royal Society of London B: Biological Sciences*, vol. 277, no. 1697, pp. 3087–3096, 2010.
- [5] Edward O Wilson, “Causes of ecological success: the case of the ants,” *Journal of Animal Ecology*, vol. 56, no. 1, pp. 1–9, 1987.

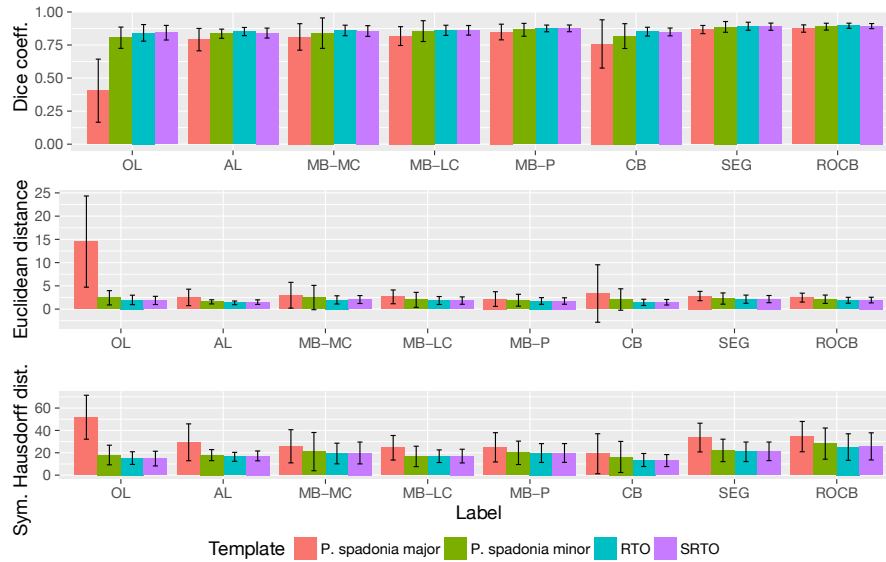


Figure 4: Evaluation of template performance per label. From top to bottom: Dice coefficient, Euclidean distance and Symmetric Hausdorff distance. Distances are expressed in microns.

- [6] Robin IM Dunbar and Susanne Shultz, “Evolution in the social brain,” *science*, vol. 317, no. 5843, pp. 1344–1347, 2007.
- [7] Wulfla Gronenberg and Andre J Riveros, “Social brains and behavior: past and present,” *Organization of insect societies: from genome to socio-complexity*, pp. 377–401, 2009.
- [8] Nicholas J Strausfeld, *Atlas of an insect brain*, Springer Science & Business Media, 2012.
- [9] Mario L Muscedere and James FA Traniello, “Division of labor in the hyperdiverse ant genus *pheidole* is associated with distinct subcaste-and age-related patterns of worker brain organization,” *PLoS One*, vol. 7, no. 2, pp. e31618, 2012.
- [10] Jürgen Rybak, “The digital honey bee brain atlas,” in *Honeybee Neurobiology and Behavior*, pp. 125–140. Springer, 2012.
- [11] James D Manton, Aaron D Ostrovsky, Lea Goetz, Marta Costa, Torsten Rohlfling, and Gregory SXE Jefferis, “Combining genome-scale *Drosophila* 3D neuroanatomical data by bridging template brains,” *bioRxiv*, p. 006353, 2014.

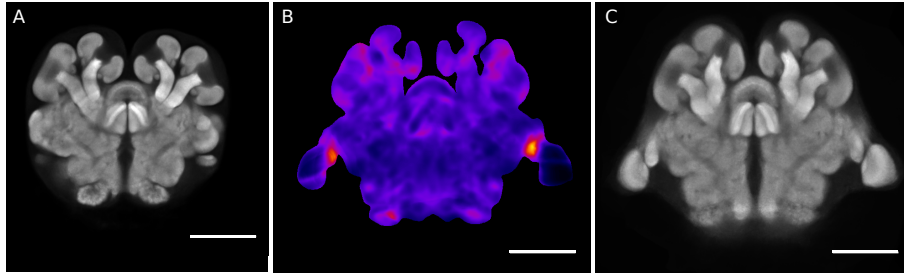


Figure 5: Inter-type deformation-based morphometry. From left to right: central view of *P. spadonia* minor template, Jacobian determinant of deformation from minor to major template, and *P. spadonia* major template. Scale bar: $100\mu\text{m}$.

- [12] Jean Talairach and Pierre Tournoux, “Co-planar stereotaxic atlas of the human brain. 3-Dimensional proportional system: an approach to cerebral imaging,” 1988.
- [13] Alan C Evans, D Louis Collins, SR Mills, ED Brown, RL Kelly, and Terry M Peters, “3D statistical neuroanatomical models from 305 MRI volumes,” in *Nuclear Science Symposium and Medical Imaging Conference, IEEE Conference Record*. IEEE, 1993, pp. 1813–1817.
- [14] John C Mazziotta, Arthur W Toga, Alan Evans, Peter Fox, and Jack Lancaster, “A probabilistic atlas of the human brain: theory and rationale for its development the international consortium for brain mapping (ICBM),” *Neuroimage*, vol. 2, no. 2PA, pp. 89–101, 1995.
- [15] X Josette Chen, Natasa Kovacevic, Nancy J Lobaugh, John G Sled, R Mark Henkelman, and Jeffrey T Henderson, “Neuroanatomical differences between mouse strains as shown by high-resolution 3D MRI,” *Neuroimage*, vol. 29, no. 1, pp. 99–105, 2006.
- [16] Belma Dogdas, David Stout, Arion F Chatziioannou, and Richard M Leahy, “Digimouse: a 3D whole body mouse atlas from CT and cryosection data,” *Physics in medicine and biology*, vol. 52, no. 3, pp. 577, 2007.
- [17] David W Shattuck, Mubeena Mirza, Vitria Adisetiyo, Cornelius Hojatkashani, Georges Salamon, Katherine L Narr, Russell A Poldrack, Robert M Bilder, and Arthur W Toga, “Construction of a 3D probabilistic atlas of human cortical structures,” *Neuroimage*, vol. 39, no. 3, pp. 1064–1080, 2008.
- [18] Gregory SXE Jefferis, Christopher J Potter, Alexander M Chan, Elizabeth C Marin, Torsten Rohlfing, Calvin R Maurer, and Liqun Luo, “Comprehensive maps of *Drosophila* higher olfactory centers: spatially segre-

- gated fruit and pheromone representation,” *Cell*, vol. 128, no. 6, pp. 1187–1203, 2007.
- [19] Jai Y. Yu, Makoto I. Kanai, Ebru Demir, Gregory S.X.E. Jefferis, and Barry J. Dickson, “Cellular organization of the neural circuit that drives *Drosophila* courtship behavior,” *Current Biology*, vol. 20, no. 18, pp. 1602 – 1614, 2010.
- [20] Sebastian Cachero, Aaron D Ostrovsky, Y Yu Jai, Barry J Dickson, and Gregory SXE Jefferis, “Sexual dimorphism in the fly brain,” *Current Biology*, vol. 20, no. 18, pp. 1589–1601, 2010.
- [21] Marta Costa, James D. Manton, Aaron D. Ostrovsky, Steffen Prohaska, and Gregory S.X.E. Jefferis, “NBLAST: Rapid, sensitive comparison of neuronal structure and construction of neuron family databases,” *Neuron*, vol. 91, no. 2, pp. 293 – 311, 2016.
- [22] Edward O Wilson, “Ants of the dominican amber (hymenoptera: Formicidae). 3. the subfamily dolichoderinae,” *Psyche*, vol. 92, no. 1, pp. 17–38, 1985.
- [23] Swidbert R Ott, “Confocal microscopy in large insect brains: zinc-formaldehyde fixation improves synapsin immunostaining and preservation of morphology in whole-mounts,” *Journal of neuroscience methods*, vol. 172, no. 2, pp. 220–230, 2008.
- [24] Brian B Avants, Charles L Epstein, Murray Grossman, and James C Gee, “Symmetric diffeomorphic image registration with cross-correlation: evaluating automated labeling of elderly and neurodegenerative brain,” *Medical image analysis*, vol. 12, no. 1, pp. 26–41, 2008.
- [25] Brian B Avants, Nicholas J Tustison, Gang Song, Philip A Cook, Arno Klein, and James C Gee, “A reproducible evaluation of ANTs similarity metric performance in brain image registration,” *Neuroimage*, vol. 54, no. 3, pp. 2033–2044, 2011.
- [26] David Legland, Ignacio Arganda-Carreras, and Philippe Andrey, “MorphoLibJ: integrated library and plugins for mathematical morphology with ImageJ,” *Bioinformatics*, p. btw413, 2016.